Evaluation of Invasiveness by Breakdown Phenomena of Electrically Induced Bubbles for a Needle-Free Injector

Keita Ichikawa, Shingo Maeda, *Member, IEEE*, and Yoko Yamanishi, *Member, IEEE*

***Abstract*— This paper evaluates a needle-free injector using electrically induced bubbles. For a minimally invasive injector, the configuration of the bubble reservoir, which is at the tip space of the bubble injector, must be optimized because the invasiveness depends on the breakdown distance of the electrically induced bubble. [2017-0121]**

***Index Terms*— Needle-free injector, microbubble, cavitation, dielectric breakdown, plasma.**

I. Introduction

NEEDLE-SYRINGES are some of the most common equipment used for care and treatment in medical facilities, but they present various challenges related to storage, disposal, and the potential of spreading infectious illnesses [1]. However, the biggest concern is the pain patients experience when a needle is inserted. In humans, the skin generally has numerous points that cause pain called "pain points", which are located about every 1 *mm* [2]. Currently, the smallest needle-syringe has a diameter of 180 μm. Thus, there is a very high probability of stimulating a pain point, which makes many people anxious or stressed. Consequently, pain from a needle injection can be a serious burden, especially for patients requiring daily insulin injections for diabetic treatment.

A potential solution to the aforementioned challenges is a needle-free injector. Current needle-free injector systems include using a pressurized gas or spring mechanism to push a drug deep inside the skin [3]. However, needle-free injector systems are not widely used and have some drawbacks, including difficulty adjusting the injection position, variability in the amount of a drug injected, and uncontrollability of the precise depth during drug injection. Although the hardness of each injection target skin varies, needle-free injectors deliver reagents at a constant pressure, making it impossible to adjust to an individual target. Similar to needle-syringes, the biggest concern is inducing pain due to position adjustment errors [4]. Another needle-free injector system used in the U.S. is to apply the force of a coil spring to create high speed water current to perforate the target to deliver a drug. This method is already used for influenza vaccinations, but some patients complain about pain, demonstrating that issues remain [5].

This research aims to develop an easy-to-use needle-free injector system that can deliver reagents with minimally-invasive stimulating a pain point by creating a minute perforation that can adjust to skin hardness. Ideally, the system will deliver reagents similar to a needle-syringe with minimal pain. Our target value of perforation diameter is less than 100 μm because perforation diameter of the conventional needle free injector is about more than 100 μm.

Because our device uses high voltage, high invasion occurs to target by plasma due to dielectric breakdown. In this paper, we measured threshold distances to avoid this invasion.

We expect that this research will have a major influence on society for the prevention of infectious illnesses and medical accidents.

II. Bubble Injector

This paper studies the bubble injector developed by our research group, which uses the collapse phenomenon of microbubbles induced by electrical field in a fluid to perforate the skin. Our device is a needle-free injection system using microbubble which has never existed before, and it is possible to achieve smaller perforation diameter compared to conventional injectors.

A. Bubble Generating, Perforation and Application Theory

Figure 1 shows the overall bubble injector and diagram of microbubble perforation. Figure 2 shows microbubble images from generation to collapse captured using a bubble injector with a copper wire by a high-speed camera (HPV-X, Shimadzu Corporation).

When high frequency pulse voltage is applied electrode which has sharp tip, high electrical field is generated by electric field concentration. This electrical field causes microscopic plasma at the tip of electrode. The plasma generation causes rising temperature at microscopic area. It occurs during thermalization of the energy carried by the free electrons. The interval time of rising temperature is much shorter

Manuscript received May 30, 2017; revised November 14, 2017; accepted December 17, 2017. Date of publication February 8, 2018; date of current version April 2, 2018. This work was supported by the Japan Society for the Promotion of Science KAKENHI under Grant JP16H04307 and Grant JP17K18857, and in part by the Japan Agency for Medical Research and Development under Grant JP17hm0102049. Subject Editor O. Tabata. *(Corresponding author: Keita Ichikawa.)*

K. Ichikawa and S. Maeda are with the School of Mechanical Engineering, Shibaura Institute of Technology, Tokyo 135-8548, Japan (e-mail: md16008@shibaura-it.ac.jp; maeshin@shibaura-it.ac.jp).

Y. Yamanishi is with the School of Mechanical Engineering, Kyushu University, Fukuoka 819-0395, Japan (e-mail: yoko@mech.kyushu-u.ac.jp).

Color versions of one or more of the figures in this paper are available online at http://ieeexplore.ieee.org.

Digital Object Identifier 10.1109/JMEMS.2018.2793314

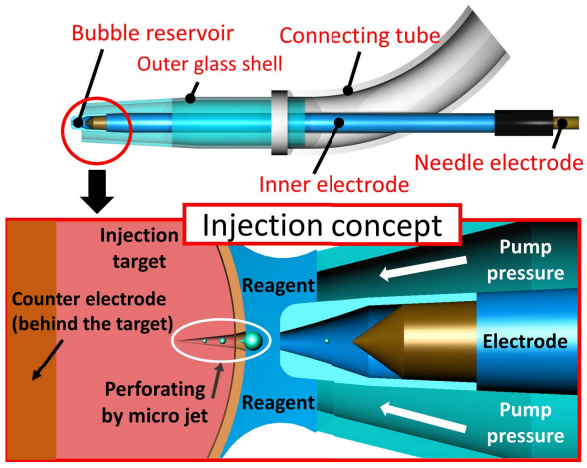

Fig. 1. The overall bubble injector and diagram of microbubble perforation.

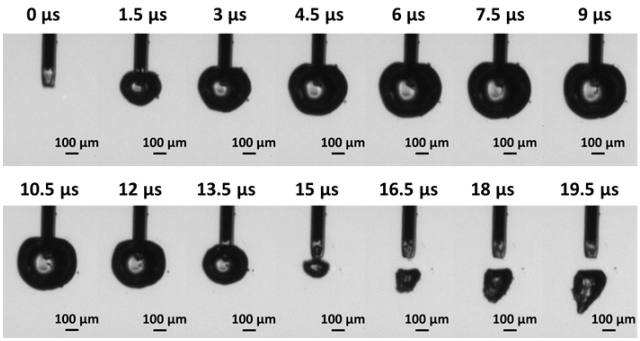

Fig. 2. Flow conditions of cavitation and a microjet.

than the acoustic transit time and acoustic relaxation do not caused during thermalization time. According to this fact, thermoelastc stress caused by temperature rise abides in thermalized volume, leading to a maximum pressure rise. This thermal elasticity generates cavitation bubble induced in the region of the tip of electrode [6]. In the case of bubble injector, by providing high frequency pulsed voltage to the bubble-generating electrodes, the surrounding liquid generates microbubbles from hydrogen and oxygen. Electrolysis and pyrolysis are also considered generating microbubbles. However, we have confirmed that the microbubble is generated both of applied high frequency DC and AC voltage at the bubble injector. Hence it can be said that the microbubble did not generated by electrolysis. In addition, FEM analysis confirmed that the temperature keeps below the threshold level where the water is thermally decomposed directly by the applied pulse voltage of used power supply. Consequently, it can be said that the microbubble is not generated by electrolysis and pyrolysis. We consider that the microbubble is generated by focusing the electric charge on the tip of electrode. In other words, the bubble injector generates the micro bubble caused by the thermal elasticity of the electrically-induced plasma. Table 1 summarizes each factors concerning electrolysis, thermal decomposition, and plasma, which are considered as possibilities of bubble generating mechanism of the bubble injector.

TABLE I
SUMMARY OF EACH FACTOR

	Thermal decomposition	Electrolysis	plasma
DC voltage	○	○	○
AC voltage	○	×	○
Pulse width	-	△ (more than 1 μm)	○
Gas species	H_2, O_2	H_2, O_2	H_2O, H_2, O_2
temperature	×	-	○

These microbubbles are pushed out from the bubble reservoir, grow quickly at the tip of the reservoir, and then collapse after reaching the maximum diameter as if shrinking. The bubble injector used in this experiment produces microbubbles that grow to a maximum diameter of approximately 300 μm. The entire process from generation to collapse takes about 20 μs. In addition, we confirmed the size of microbubbles become smaller by using electrode with smaller diameter and lower applied voltage. The collapse of microbubbles causes a non-uniform shrinkage, resulting in a high-speed water flow called a microjet. This water flow penetrates inside the bubbles, and flows in the direction of bubble progression. The collapsed bubbles are consequently injected forward due to the inertial force of the microjet. The jet pressure at the moment a microbubble collapses generally exceeds $1GPa$. Hence, the high pressure of a microjet in a bubble injector can be used to perforate the skin [7]. Figure 3 shows sequence pictures that the microbubble which is generated and ejected by the bubble injector, and then it is collapsed. After that it was observed that the microjet is penetrated into the agarose gel. We confirmed that the microbubble is swelled as soon as after its generation. After that it is collapsed and caused microjet. The microjet pierced into the gel surface as shown in Figure 3.

B. Manufacturing Method of Bubble Injector

Figure 4 shows Cu wire with a diameter of 100 μm is placed inside a micropipette glass tube (external diameter 1.37 mm, inner diameter 0.93 mm). Then the glass tube is pulled and cut using a weight with a glass tube puller (PC-10, Narishige Group) while heating. Due to the viscosity difference between the glass tube and the Cu wire, the glass becomes longer than the Cu wire. By processing the tip of this glass tube using a microforge (MF-900, Narighige Group) into a length of approximately 150 μm, a bubble-generating electrode can be created. The produced bubble-generating electrode needs to be connected to a tungsten needle electrode using a Ag paste. Next to produce a shell that holds the reagent supply, the micropipette glass tube (external diameter 2.03 mm, inner diameter 1.68 mm) must be pushed into a pipette tip with an inner diameter of 500 μm and glued with an adhesive. After that, the bubble-generating electrode and the reagent supply shell are temporarily attached with a connecting tube with an inner diameter of 2 mm. Then the bubble-generating electrode's tip must be adjusted to be approximately 100 μm

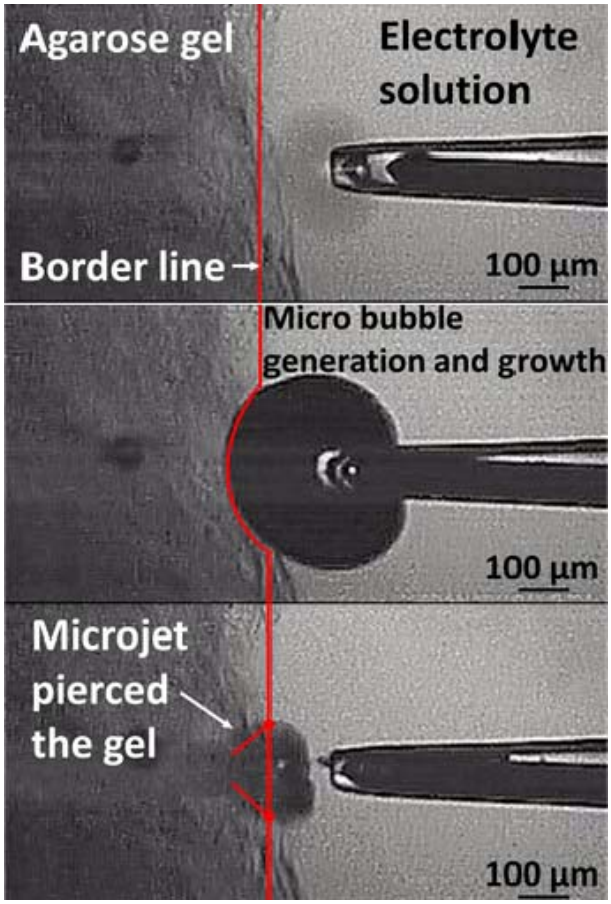

Fig. 3. Sequence photos of perforating agarose gel surface by microbubble.

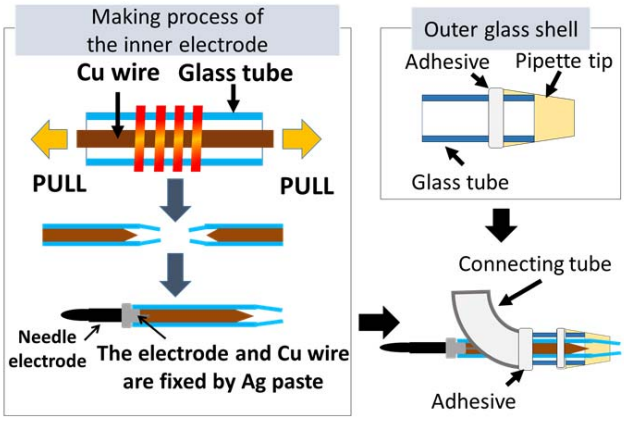

Fig. 4. Process flow to fabricate the bubble injector.

outside the reagent supply shell. After finalizing the position, adhesive is used to permanently secure the joints between the connecting tube, bubble-generating electrode, and reagent supply shell, completing the injector. Figure 5 shows the bubble injector which we made actually.

It is important to note that our device is a simple fabrication process with low cost that is only using pulling glass capillary/metal with simple assembling processes.

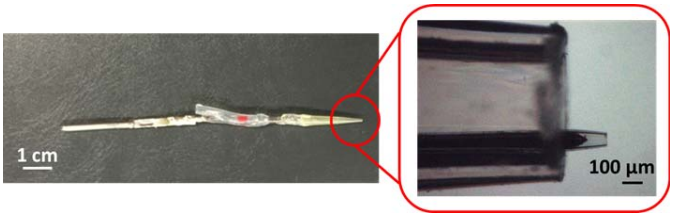

Fig. 5. Image of the bubble injector.

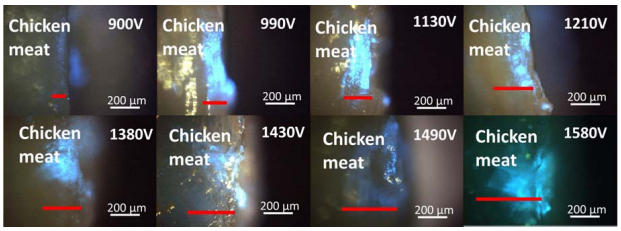

Fig. 6. Increase in the injection region as a function of the input power (red lines indicate injection depth).

C. Perforatability and Existing Issues

Figure 6 shows the real-time images by high-speed camera for injecting reagent to chicken meat. The reagent is mixed fluorescent beads (Thermo company, Flouro-Max, diameter is 2.1 μm) and normal saline solution. The reagent was injected under condition that the distance between the bubble injector and the chicken meat was 50 μm. The blue shiny areas are the fluorescent reagent injection region. The ability of perforation is confirmed by applying an input voltage. Furthermore, the ability of perforation is increased as the input voltage increases. However, along with the increase in the input voltage, dielectric breakdown of bubbles occurs between the bubble-generating electrode and the perforation target (Figure 7), causing a high invasiveness due to plasma generation. Avoiding plasma generation is necessary because implementing a bubble injector as a needle-free injector system for a practical use requires minimal invasiveness as well as stable and repeatable reagent delivery.

III. Experiment to Measure the Distance of Plasma

A. Purpose and Design of the Experiment

The bubble injector uses electrical discharges in a liquid to generate microbubbles. As stated previously, plasma is formed during the electrical discharge due to dielectric breakdown, leading to the invasiveness to the perforation target surface. Therefore, it is necessary to determine the range of distances between the bubble injector and the object, which avoid plasma-causing invasiveness.

In this experiment, swine skin was used as a target. The parameters used were the distance from the bubble injector and the output voltage from the power supply. The plasma generating distance at each output was measured.

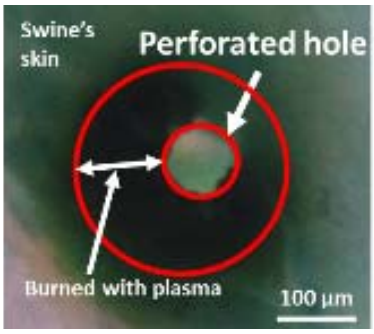

Fig. 7. Example of a high-invasive ablation to porcine skin by plasma-cavitation (applied voltage is about 1200 V).

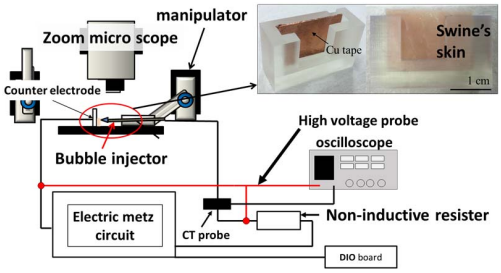

Fig. 8. Experimental setup to evaluate the distance of initial plasma irradiation.

B. Overview of the Setup

Figure 8 overviews the experimental device setup. To avoid damaging the device due to a high electric input current, a 7.48-kΩ non-inductive resistor was added, and the bubble-generating electrode, shown as the part bent in the middle in Fig. 5, was connected to the hyfrecator 2000 (ConMed Corporation), which is a power supply used as a medical apparatus for an electric scalpel, whose characteristics are detailed in the next section. The bubble-generating electrode connected to the power supply is secured to the right arm of the micromanipulator (QP-2RLH-PC, Micro Support Co., Ltd.). A 0.9% NaCl liquid was provided through the reagent supply shell. A liquid surface was created to cover the swine skin (2-*mm* thick), which was fastened with the jig to act as the counter electrode, and the tip of the bubble-generating electrode. To minimize the measurement errors and to ensure that the object was vertical to the microscope, the jig to secure the target object was created using a 3D printer (form 2, Formlabs Inc.). The manipulator could adjust the distance between the swine skin and the bubble generating electrode. A real-life zoom microscope and CCD camera were used to measure the distance. Plasma generation was determined by the light emission of plasma visible through the microscope as well as the sharp increase in the electric current observed by the oscilloscope (TPS2024B, Tektronix inc.) and the CT probe (3276, Hioki Co., Ltd.) because the jump phenomenon, which is the sharp increase in the electric current when a high frequency plasma is generated, is known to occur [8].

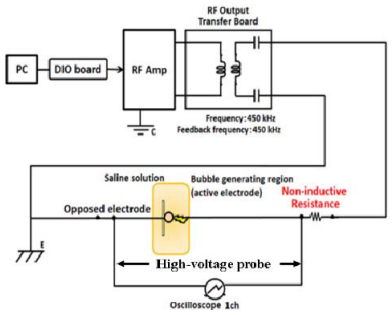

Fig. 9. Electric circuit diagram of the measuring waveform of the power supply.

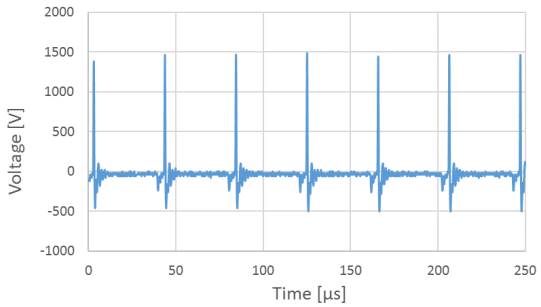

Fig. 10. Measured waveform of the output voltage.

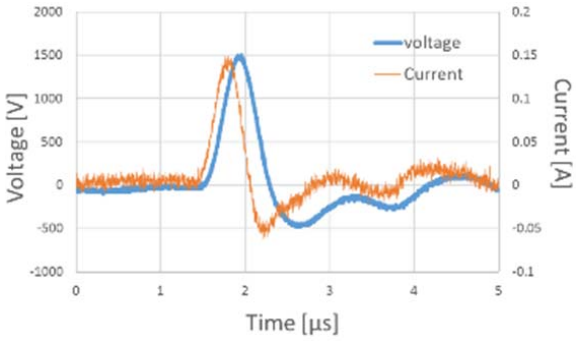

Fig. 11. Relationship between the voltage and current at power supply over time.

C. Power Supply: Medical Apparatus Used in Electrosurgery

The hyfrecator 2000 is a power supply used in electrosurgery. Figure 9 shows the electrical circuit diagram. The output waveform obtained from the oscilloscope connected to the electric circuit using the bubble-generating electrode is the active electrode.

Figure 10 is the measured waveform before a plasma is formed, while Fig. 11 shows enlarged graphs of a single pulse of both the voltage and electric current as functions of time. The power supply used in this experiment provides a damped sine wave voltage with a frequency of 450 *kHz*, 600 pulses for a single output. Because the output is controlled by the constant value of power, it supplies the appropriate voltage and current for the power. Figure 10 shows slight variabilities in the maximum voltage in the pulse for a constant output.

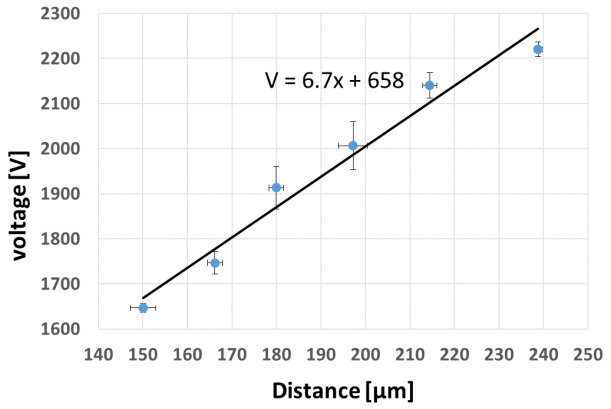

Fig. 12. Distance required to generate a plasma as a function of applied voltage.

D. Method

In the experiment, the real-life zoom microscope was initially positioned to focus on the bubble-generating electrode and the cross-section of the swine skin. Then the bubble-generating electrode was moved gradually towards the swine skin using a micromanipulator controlled by a computer while a high-frequency power supply provided the output in one-second intervals. The movement was terminated when plasma generation was confirmed, and the arm location of the micromanipulator was adjusted slightly by changing distance between the swine skin and the bubble-generating electrode to determine the precise location of plasma generation. Once the electrode's position was determined, the voltage and current were measured using the oscilloscope and the distance between the swine skin and the tip of the bubble-generating electrode were measured from the computer monitor. For each output, measurements were repeated thrice and the average was used as an experimental value between electrode and object for the applied voltage.

IV. Experimental Results and Analysis

A. Experimental Results

Figure 12 shows the experimental results. The plasma-generating distance is linear with the applied voltage. Additionally, the graph shows the variability of the voltage for each output due to the characteristics of the power supply used in this experiment; the voltage of the power supply varies within a certain range for the output. The difference between the linear fit and the measurement results is attributed to error factors such as manually adjusting the final position using the manipulator and measuring from the computer monitor as well as factors related to the power supply used in the experiment.

As for the factors caused by the power supply, the following mechanism can influence the measurement results; for each output, a 600 high-frequency pulse voltage is applied, initiating the moment when a microbubble is grown and ready to be released from the bubble-generating electrode. The next pulse input creates a new microbubble, which causes these two microbubbles to become too close, resulting in dielectric breakdown. This behavior influences the measurement results.

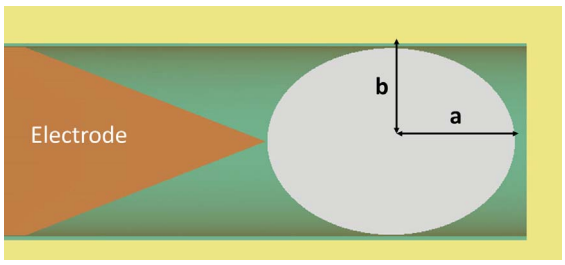

Fig. 13. Model of a microbubble to calculate the theoretical value of breakdown.

To avoid this issue, it is necessary to develop a power supply that produces the same output waveform as the one used in this experiment, but supplies a given number of pulses at select frequencies.

From the linear relationship between the applied voltage and the distance obtained from this experiment, we compared and analyzed using the theoretical value derived from the equation of dielectric breakdown in the subsequent section.

B. Theoretical Equation of Dielectric Breakdown

The electric field E_i in a liquid **micro bubble** can be expressed as [9]

$$E_i = \frac{E_o}{1 + \frac{ab^2}{2\varepsilon_w}(\varepsilon_b - \varepsilon_w) \times \frac{1}{a^3b^3}(-2e + ln\frac{1-e}{1+e})} \tag{1}$$

$$\mathrm{e} = \sqrt{1 - \frac{b^2}{a^2}} \tag{2}$$

where E_0 is the external electric field, ε_w is the dielectric constant of a 0.9% NaCl liquid (relative permittivity of 80), and ε_b is the dielectric constant of oxygen (relative permittivity of 1). As shown in Fig. 13, a and b are the length of major and minor axes of a microbubble. The external electric field E_0 can be expressed using d, which is the distance between the bubble-generating electrode and the target object, and the applied voltage V as

$$E_o = \frac{V}{d} \tag{3}$$

Substituting equation (1) with equation (3) and reorganizing the equation in terms of the electrode distance d, gives

$$\mathrm{d} = \frac{1}{1 + \frac{ab^2}{2\varepsilon_w}(\varepsilon_b - \varepsilon_w) \times \frac{1}{a^3b^3}(-2e + ln\frac{1-e}{1+e})} \cdot \frac{V}{E_i} \tag{4}$$

Moreover, the dielectric strength of air is $E_{max} = 3V/\mu m$. Exceeding this value may cause dielectric breakdown to generate plasma discharges [10], [11]. Therefore, the value in equation (4) using $E_i = E_{max}$ becomes the plasma-generating distance.

The size of each elliptical microbubble was measured from the image captured by the high-speed camera (VW-9000, KEYENCE CORPORATION). In this experiment, the minor axis b of a microbubble is considered to be constant because it was restricted by the wall of the glass tube. As a microbubble is generated by electrically induced due to the applied voltage

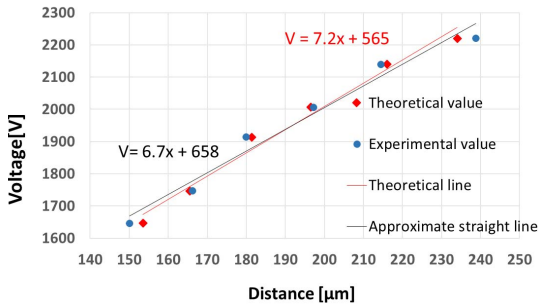

Fig. 14. Comparison of the experimental and theoretical values of breakdown.

in the major axis direction, the major axis a, whose size depends on the output value, was measured.

C. Comparison of Theoretical and Experimental Values

Figure 14 shows the theoretical and experimental values of the dielectric breakdown in liquid microbubbles for each output. For each applied voltage, the theoretical and experimental values agree well. The difference between the angles of the slopes between the linear fit for the experimental values and theoretical line is only about 0.5 μm that occurs around 1 V, showing a very high fit. Although the experimental values deviate from the theoretical values, the maximum difference is only about 5 μm, which is minute. We believe this difference is caused by the accumulation of measurement errors in the distance to the target object and the length of the major axis a. On the other hand, the difference between the intercept against the voltage axis is approximately 100 V and cannot be ignored. We anticipate a larger difference between the theoretical and experimental values for the range of applied voltage outside of this experiment.

The experimental values of the plasma generating threshold distances are valid in the applied voltage range of $1600 \sim 2300$ V. To obtain the theoretical values for the range below 1600 or above 2300 V, similar experiments with a broader range of applied voltages should provide a better approximation line as well as the theoretical line for bubble injectors. Using this experiment as a model, future reagent injection experiments using bubble injectors can employ the same type of device and measure the generated microbubble size for each output to obtain the estimated distance for plasma generation using equation (4). Hence, target indicators for reducing the invasiveness of a bubble injector can be acquired from theoretical equations.

V. Conclusion

We focus on microbubbles induced by electrical fields to develop a new needle-free injector system, and implement the target perforation method using the cavitation phenomenon. We confirm the perforatability and injectability of a reagent using this method while identifying the issue of high invasiveness due to plasma generation by dielectric breakdown in a fluid discharge in bubble injectors. To avoid invasiveness, this experiment measured the plasma generating threshold distance from the actual discharge and obtained reference values of distance from the target for the usage of bubble injectors. A linear relationship is revealed between the dielectric breakdown distance and applied voltage for the bubble injector. Additionally, the distance increases to 6.7 μm for a 1-V increase in the applied voltage.

By rewriting the theoretical equation of dielectric breakdown in terms of the distance between electrodes, the theoretical value is obtained for each applied voltage using the measured elliptical microbubble size. These values are compared to the experimental ones. The maximum difference between the theoretical and experimental values is 5 μm, which is considered to be negligible, validating the experimental results. Moreover, measuring the size of an elliptic microbubble generated by the applied voltage in a bubble injector can theoretically estimate the dielectric breakdown. The application example in Fig. 6 shows a distance between the bubble injector and the target object of 50 μm, but to avoid invasiveness from the plasma, the distance must be approximately 150 μm. However, the increased distance between the device and the target object may reduce the perforatability and injectability of reagent.

Future research plans should include the development of a power supply capable of controlling the number of pulses and the frequency for each output with a waveform similar to the electro surgery power supply used in this study. Additionally, experiments involving a wider range of applied voltages should be conducted to reveal the threshold distance of the dielectric breakdown occurrence in bubble injectors and we will perform some experiments that confirming the effects of reagent, skin and water/ion contents. Furthermore, to improve bubble injectors for practical applications, further experiments must be carried out, including actual reagent injection experiments using theoretical estimations of the dielectric breakdown distance and assessments of injectability of reagents by avoiding plasma-causing high-invasiveness. In addition, we confirmed that the microbubble is generated wherever counter electrode is located in circuit. A new device is under development that avoid applying high voltage between skin and injector by mounting a counter electrode inside, so that the electric current hardly flows to the target side.

Acknowledgment

In this study, we are grateful to Mr. Moriizumi of BEX Inc. for valuable advices about high frequency pulse etc.

References

[1] N. Takahashi, "SAFETY4-what design can do for social issues proposal for safely disposable needle-syringes," *Des. Res.*, vol. 56, p. 60, 2011.
[2] S. Aoyagi, "Visualization in development of microneedle—Development of painless needle imitating mosquito," *J. Vis. Soc. Jpn.*, vol. 33, pp. 145–148, Oct. 2013.
[3] C. L. C. Chase, C. S. Daniels, R. Garcia, F. Milward, and T. Nation, "Needle-free injection technology in swine: Progress toward vaccine efficacy and pork quality," *J. Swine Health Prod.*, vol. 16, no. 5, pp. 254–264, 2008.
[4] E. L. Giudice and J. D. Campbell, "Needle-free vaccine delivery," *Adv. Drug Del. Rev.*, vol. 58, no. 1, pp. 68–89, 2006.

[5] N. Petrovsky, Y. Honda-Okubo, M. Royals, K. Bragg, and D. Sajkov, "A randomized controlled study to assess the immunogenicity and tolerability of a 2012 trivalent seasonal inactivated influenza vaccine administered via a disposable syringe jet injector device versus a traditional pre-filled syringe and needle," *Trials Vaccinol.*, vol. 2, pp. 39–42, Dec. 2013.

[6] A. Vogel, J. Noack, G. Hüttman, and G. Paltauf, "Mechanisms of femtosecond laser nanosurgery of cells and tissues," *Appl. Phys. B, Lasers Opt.*, vol. 81, no. 8, pp. 1015–1047, 2005.

[7] H. Kato, *New Edition Cavitation Basics and Recent Development (Kyabitēshon Kiso to Saikin no Shimpo)*. Tokyo, Japan: Morikita, 2016, p. 203.

[8] A. S. Bugaev, V. I. Gushenets, A. G. Nikolaev, E. M. Oks, and G. Y. Yushkov, "Influence of a current jump on vacuum arc parameters," *IEEE Trans. Plasma Sci.*, vol. 27, no. 4, pp. 882–887, Aug. 1999.

[9] M. Kurahashi, S. Katsura, and A. Mizuno, "Basic Study on Discharge inside Bubbles in Water," *J. Inst. Electrostat. Jpn.*, vol. 20, no. 6, pp. 357–363, 1996.

[10] H. Okubo *et al.*, "Handbook for electrical discharge first volume (Hōden handobukku Jōkan)," in *Committee for Handbook for Electrical Discharge (hōden Handobukku Shuppan Iinkai)*. Tokyo, Japan: Ohmsha 1998, pp. 262–264.

[11] S. Menju and K. Takahashi, "DC dielectric strength of a SF_6 gas insulated system," *IEEE Trans. Power App. Syst.*, vol. PAS-97, no. 1, pp. 217–224, Jan. 1978.

Authors' photographs and biographies not available at the time of publication.